Numerical analysis of dislocation density and residual strain in multicrystalline silicon for solar cells using experimental verification

Nakano, Satoshi
Research Institute for Applied Mechanics, Kyushu University

Gao, Bing
Research Institute for Applied Mechanics, Kyushu University

Jiptner, Karolin
National Institute for Materials Science

Harada, Hirofumi
National Institute for Materials Science

他

https://doi.org/10.15017/1660355

出版情報：九州大学応用力学研究所所報. 150, pp.1-5, 2016-03. Research Institute for Applied Mechanics, Kyushu University
バージョン：
権利関係：

Numerical analysis of dislocation density and residual strain in multicrystalline silicon for solar cells using experimental verification

Satoshi NAKANO[*1], Bing GAO[*1], Karolin JIPTNER[*2], Hirofumi HARADA[*2], Yoshiji MIYAMURA[*2], Takashi SEKIGUCHI[*2], Masayuki FUKUZAWA[*3] and Koichi KAKIMOTO[*1]

E-mail of corresponding author: *snaka@riam.kyushu-u.ac.jp*

(Received January 7, 2016)

Abstract

A three-dimensional (3D) Haasen-Alexander-Sumino model (HAS model) has been developed to study the dislocation density and residual strain in the crystal. We compared the difference between calculation results and experimental results. The results show that the HAS model can evaluate the dislocation density and residual strain in the crystal semiquantitatively. And the residual strain for a multicrystal is lower than that for a mono-like crystal, while the dislocation density for the multicrystal is higher than that for the mono-like crystal. In the case of mono-like crystal, the dislocation generation is small and the thermal stress cannot relax easily, then residual strain is high. In the case of the multicrystal, the dislocation generation is large and there are so many grains, then the thermal stress can relax easily and residual strain is low.

Keywords : *Silicon, Solar cell, Directional solidification, Dislocation, Strain*

1. Introduction

In recent years, photovoltaic energy is essential to solve the energy issues and environmental problems which we confront. For widespread utilization of the photovoltaic application in the world, it is important to fulfill the demand of cost reduction and improvement of conversion efficiency. The directional solidification method is important and most prevailing method for growing multicrystalline silicon (mc-Si) ingots for photovoltaic materials. Major advantages of this method are low cost and high throughput for photovoltaic production. However, seeded directional solidification method (seed-cast)[1-3] has been a focus of constant attention. Mono-like Si ingots are grown from seed crystals, which are putted at the bottom of the crucible using the directional solidification method. These days, the conversion efficiency of mono-like Si is about the same that of monocrystalline Si, which is grown by the Czochralski (CZ) method[4]. For mc-Si or mono-like Si, which is grown by the directional solidification method, it is widely known that high dislocation density is main problem to decrease conversion efficiency[5, 6], while residual stress can cause the crystals to fracture[7, 8]. For increasing both conversion efficiency and yield rate of solar cells, the dislocation density and residual stress in the crystal needs to be improved.

For experimental method, it is important to evaluate the quality of crystals [9-12], but this cannot be estimated how to generate dislocation and residual stress during the growth process. Numerical simulation is a powerful tool to provide us a valuable perception by analyzing calculation results of the crystal during the growth process. Therefore, we can improve the furnace design and optimize the growth condition, which are effective to the quality of the crystal, by numerical simulation.

A 3D Haasen-Alexander-Sumino model (HAS model) has been developed[13-17] to study the behavior of dislocation and residual strain during the growth process. We assumed the silicon crystal was isotropic, crystal anisotropy was neglected. In this study, we pay attention to the HAS model can be used to calculate dislocation density and residual strain for mono-like Si and mc-Si even we assumed the silicon crystal was isotropic. And

*1 Research Institute for Applied Mechanics, Kyushu Univ.
*2 National Institute for Materials Science
*3 Kyoto Institute of Technology

we analyzed the relationship between the dislocation density and residual strain using this model.

2. Computation Method

The directional solidification furnace consisted of a silicon melt, a crystal, crucibles, pedestals, heat shields, and heaters. The crystal had a height of 75 mm and a diameter of 105 mm.

A transient global model was developed for the directional solidification process to investigate the global heat transfer in the entire furnace as a function of time. Global heat transfer in the entire furnace included the convective heat transfer of the silicon melt, the conductive heat transfer in all of the solid components, and the radiative heat transfer in all of the diffusive surfaces of the furnace. A dynamic interface tracking method was also included to obtain the shape of the solid–liquid interface. Details of the calculations have already been reported elsewhere[18-20].

A 3D HAS model was also investigated using the temperature distributions in the crystal which we calculated. A brief explanation of the formulas as follows. Details of the calculations can be found elsewhere[13-17].

A silicon crystal has twelve slip directions because of its fcc structure[17, 21]. The resolved shear stress $\tau^{(\alpha)}$ in the α slip direction can be obtained using the tensor transformation technique[21]. The creep strain rate is obtained by Orowan's relationship as follows[22]:

$$\frac{d\varepsilon_{pl}^{(\alpha)}}{dt} = N_m^{(\alpha)} v^{(\alpha)} b \tag{1}$$

where N_m is the mobile dislocation density, b is Burger's vector, and v is the slip velocity of the dislocation.

The rate of the mobile dislocation density in the α slip direction is given as follows:

$$\frac{dN_m^{(\alpha)}}{dt} = KN_m^{(\alpha)} v^{(\alpha)} \tau_{eff}^{(\alpha)} + K^* N_m^{(\alpha)} v^{(\alpha)} \tau_{eff}^{(\alpha)} \sum_{\beta \neq \alpha} f_{\alpha\beta} N_m^{(\beta)} - 2r_c N_m^{(\alpha)} N_m^{(\alpha)} v^{(\alpha)} \tag{2}$$

where τ_{eff} is the effective stress for dislocation multiplication, K and K^* are multiplication constants[15-17], and r_c is the effective dipole half width[15-17]. The $f_{\alpha\beta}$ coefficients are given either as one or zero.

The slip velocity of the dislocation v is given by:

$$v^{(\alpha)} = v_0 \left(\frac{\tau_{eff}^{(\alpha)}}{\tau_0}\right)^m \exp\left(-\frac{U}{k_b T}\right) \tag{3}$$

where $v_0 = 5000 m/s$, $\tau_0 = 1 MPa$, $m = 1$, $U = 2.2 eV$, $k_b = 8.617 \times 10^{-5} eVK^{-1}$ [23]. The effective stress is given by:

$$\tau_{eff}^{(\alpha)} = \left\langle \tau^{(\alpha)} - \tau_i^{(\alpha)} - \tau_b^{(\alpha)} \right\rangle \tag{4}$$

where $\tau^{(\alpha)}$ is the resolved shear stress, $\tau_i^{(\alpha)}$ is the stress for overcoming short-range obstacles, and $\tau_b^{(\alpha)}$ is the internal long-range elastic stress which is caused by mobile dislocations[15-17, 23].

The short-range and long-range interactions are given as follows[23]:

$$\tau_i^{(\alpha)} = \mu b \sqrt{\sum_\beta a_{\alpha\beta} (N_m^{(\beta)} + N_i^{(\beta)})} \tag{5}$$

$$\tau_b^{(\alpha)} = \mu b \sum_\beta A_{\alpha\beta} \sqrt{N_m^{(\beta)}} \tag{6}$$

where $a_{\alpha\beta}$ and are $A_{\alpha\beta}$ the interaction coefficients[23].

Because the dislocation densities and creep strains for all of the slip directions are obtained, the total dislocation density and total creep strain can be expressed as:

$$N_m = \sum_{\alpha=1}^{12} N_m^{(\alpha)} \tag{7}$$

$$\boldsymbol{\varepsilon}_{pl} = \sum_{\alpha=1}^{12} \boldsymbol{\varepsilon}_{pl}^{(\alpha)} \frac{1}{2} (\mathbf{n}^{(\alpha)} \otimes \mathbf{m}^{(\alpha)} + \mathbf{m}^{(\alpha)} \otimes \mathbf{n}^{(\alpha)}) sign(\tau^{(\alpha)}) \tag{8}$$

where $\mathbf{n}^{(\alpha)}$ is the normal unit vector of the slip plane and $\mathbf{m}^{(\alpha)}$ is the unit vector of the slip direction.

The following assumptions were made: (1) the boundary condition at the solid–liquid interface was a no traction boundary, and (2) the boundary conditions at the crystal-crucible wall interfaces were also no traction boundaries because a coating was used between the silicon melt and the quartz crucible in order to reduce the effect of the crucible.

3. Results and discussion

We used one of major crystal growth methods based on the directional solidification process; the traveling heater method. In the traveling heater method, the heaters were moved upward in order to grow the crystal, while the heater power was held constant until completion of the solidification process, at which point it was decreased.

Two mono-like crystals (Crystal 1 and Crystal 2) were grown by the traveling heater method using (001)-oriented seed crystals[10, 11]. Figure 1 shows the growth recipe of heater temperature and crucible position for the experiment[11]. We conformed to the melting and solidification process for two crystals and only changed the cooling rate during the cooling process below 900 °C. The cooling rate for Crystal 1 was about 12 °C/min, whereas that for Crystal 2 was about 5 °C/min below 900 °C. Figures 2 (a) and 2(b) are the optical images of Crystal 1 and Crystal 2. Two ingots were cut 1.5 mm thickness at vertical direction with (110) surface to measure the dislocation density and residual strain in the ingot. Crystal 1 has a large area of mono crystal which grew from the seed crystal; however Crystal 2 has a large area of multicrystal which originated from the side wall. The measurement of residual strain was performed using a scanning infrared polariscope (SIRP). Details of the SIRP measurement can be found in publications[24, 25]. We also calculate temperature distribution in the crystal with following parameters. The cooling rate for Crystal 1 was about 6.1 °C/min, whereas that for Crystal 2 was about 2.2 °C/min below 900 °C. The cooling rate between experiment and calculation is different; however, we can verify the effect of the cooling rate below 900 °C qualitatively.

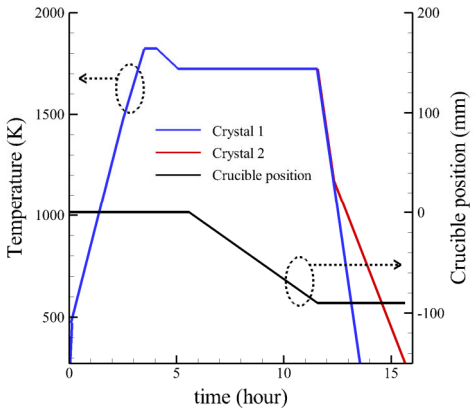

Fig. 1 The growth recipe of heater temperature and crucible position for the experiment.

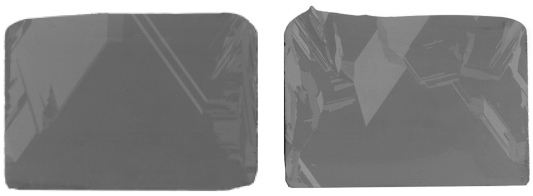

(a) (b)

Fig. 2 Optical images of (a) Crystal 1 and (b) Crystal 2.

Figure 3 shows the distribution of dislocation density in the periphery of the crystals with respect to the ingot height in the calculation results and experimental results. The previous 2D calculation results are different from the experimental results by one order of magnitude. However, our new 3D calculation results are very close to the experimental results. The calculation results for Crystal 1 and Crystal 2 are almost the same because the dislocations were mainly generated at the high-temperature region in the HAS model and because our calculations did not take into account for the dislocation propagation and movement. Therefore, the distribution of dislocation density for Crystal 1 and Crystal 2 is almost the same because the cooling rate changed at 900 °C, which is not a high-temperature region.

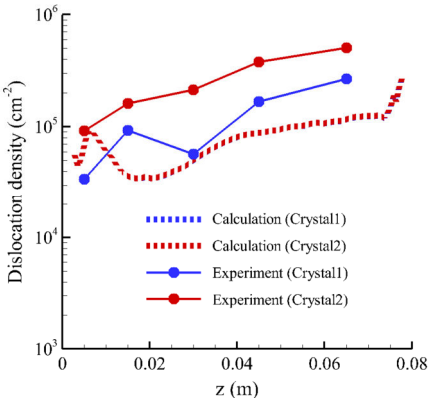

Fig. 3 The distribution of dislocation density in the periphery of the crystal with respect to the ingot height in the calculations and the experiments.

Figures 4(a) and 4(b) show SIRP images of Crystal 1 and Crystal 2[10, 11]. Figures 5(a) and 5(b) show the distribution of residual strain of Crystal 1 and Crystal 2 for calculation results. From Fig. 4(a) and Fig. 5(a), both residual strain distributions are symmetric distribution and quite similar. And the higher strain in the crystal is periphery and lower strain is in the center. These results suggest that the peripheries in the crystal are the areas of high temperature gradients and therefore the high thermal stresses are in those areas. From Fig. 2(b), 4(b) and 5(b), even multicrystal area in the ingot is large, the distribution of residual strain for calculation result is close to that for experimental result.

Figures 6(a) and 6(b) show an optical image and SIRP image of multicrystalline silicon ingot[10]. The solidification and cooling process is the same as Crystal 1. Even there are so many grains, the distribution of residual strain as shown in Fig. 5(a) is close to the SIRP image as shown in Fig. 6(b). Figures 7(a) and 7(b) show the distribution of residual strain in the center and

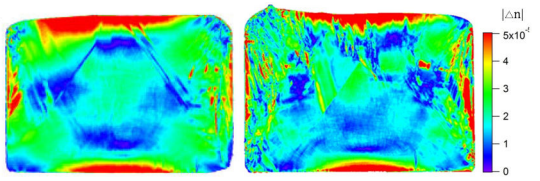

(a) (b)

Fig. 4 SIRP images of (a) Crystal 1 and (b) Crystal 2.

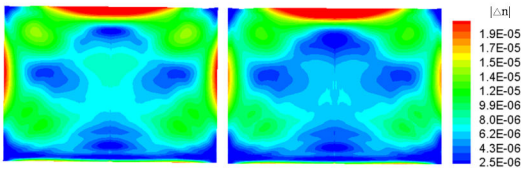

(a) (b)

Fig. 5 The distribution of residual strain in (a) Crystal 1 and (b) Crystal 2 in the calculations.

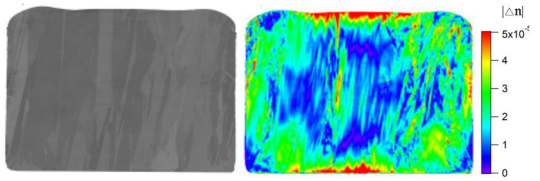

(a) (b)

Fig. 6 (a) Optical image and (b) SIRP image of the multicrystalline silicon ingot.

periphery of the crystal with respect to the ingot height for the calculation and experimental results. The distribution of residual strain for Crystal 1 and Crystal 2 in calculation result is close to that for experimental result. And the difference of residual strain between Crystal 1 and Crystal 2 is small. The distribution of residual strain for multicrystal ingot is also close to that for calculation results. And residual strain for multicrystal ingot is lower than that for mono-like ingot Crystal 1 and Crystal 2. The average dislocation density in whole of the crystal for Crystal 1, Crystal 2 and multicrystal is 0.5×10^5, 1.1×10^5, and 1.5×10^5 cm^{-2} respectively[26]. The average dislocation density for multicrystal is higher than that for mono-like Crystal 1 and 2. This phenomenon is owing to the relationship between the dislocation density and the residual strain in the crystal. For the mono-like crystal, because dislocation generation is small, thermal stress cannot easily relax and the residual strain is high. In contrast, for the multicrystal, because dislocation generation is large and there are many grains, the thermal stress can easily relax, and therefore the residual strain is low. In case of increasing the size of crystal, difference of

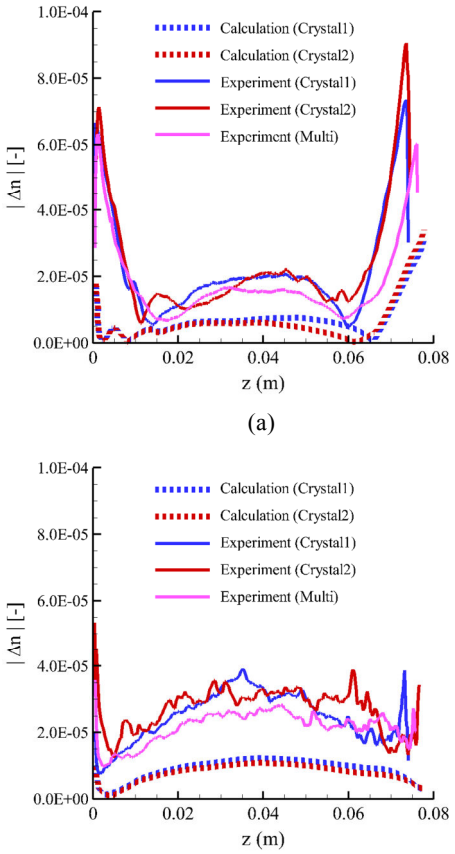

Fig. 7 The distribution of residual strain in the (a) center and (b) periphery of crystal with respect to the ingot height in the calculations and experiments.

residual strain between mono-like crystal and multicrystal could be increased. Therefore, we can expect the difference of residual strain could be more effective to dislocation density. Thus, even multicrystal area in the ingot is large, HAS model is very useful to expect the distribution of dislocation density and residual strain semiquantitatively.

4. Conclusion

A 3D Haasen-Alexander-Sumino model has been developed and compared with experimental results performed in mono-like and multicrystal silicon ingots to study the relationship between dislocation density and residual strain in the crystal. The calculation results are good agreement with the experimental results even crystal has large multicrystal area. From these results, the HAS model is very useful model to evaluate dislocation density and residual strain in the crystal semiquantitatively. And we verified the relationship between dislocation density and residual strain in the crystal using numerical analysis in comparison with

experimental results.

Acknowledgement

This work was partly supported by the New Energy and Industrial Technology Development Organization (NEDO) under the Ministry of Economy, Trade and Industry (METI).

References

1) N. Stoddard, B.Wu, I.Witting, M.Wagener, Y.Park, G.Rozgonyi, R.Clark, Solid State Phenom. 131 (2008) 1.
2) Y. Miyamura, H. Harada, K. Jiptner, J. Chen, R.R. Prakash, J.Y. Li, T. Sekiguchi, T. Kojima, Y. Ohshita, A. Ogura, M. Fukuzawa, S. Nakano, B. Gao, K. Kakimoto, Solid State Phenom., 89 (2013) 205.
3) B. Gao, S. Nakano, H. Harada, Y. Miyamura, T. Sekiguchi, K. Kakimoto, Journal of Crystal Growth, 352(1), (2012) 47.
4) Takahiro Arima, Takemichi Honma, Shin Sugawara and Yasuhiro Matsubara, 6th World Conference on Photovoltaic Energy Conversion, Kyoto, Japan, p511, 2014.
5) K. Arafune, T. Sasaki, F. Wakabayashi, Y. Terada, Y. Ohshita, M. Yamaguchi, Physica., B 376-377 (2006) 236.
6) M. M'Hamdi, E. A. Meese, E. J. Ovrelid, and H. Laux, Proceedings 20th EUPVSEC (2005) 1236.
7) S. Nakano, B. Gao, K. Kakimoto, J. Cryst. Growth, 318 (2011) 280.
8) M. M'Hamdi, S. Gouttebroze, and H. G. Fjar, J. Cryst. Growth, 318 (2011) 269.
9) Y. Miyamura, J. Chen, R. Prakash, K. Jiptner, H. Harada, T. Sekiguchi, Acta Phys. Pol. A 125[4] (2014) 1024.
10) K. Jiptner, M. Fukuzawa, Y. Miyamura, H. Harada, and T. Sekiguchi, J. J. Applied Physics, 52(2013) 065501.
11) K. Jiptner, M. Fukuzawa, Y. Miyamura, H. Harada, K. Kakimoto, and T. Sekiguchi, Physica Status Solidi C, 10 (2013) 141.
12) M. Trempa, C.Reimann, J.Friedrich, G.Muller, D.Oriwol, J.Cryst.Growth 351 (2012) 131.
13) H. Alexander, P. Haasen, Solid State Physics, 22 (1968) 27.
14) M. Suezawa, K. Sumino, I. Yonenaga, J. Appl. Phys., 51 (1979) 217.
15) B. Gao, S. Nakano, H. Harada, Y. Miyamura, K. Kakimoto, Cryst. Growth Des., 13 (2013) 2661.
16) B. Gao and K. Kakimoto, J. Cryst. Growth, 384 (2013) 13.
17) B. Gao and K. Kakimoto, J. Cryst. Growth, 396 (2014) 7.
18) L. J. Liu, S. Nakano, and K. Kakimoto, J. Cryst. Growth, 282 (2005) 49.
19) K. Kakimoto, L. J. Liu, and S. Nakano, Mater. Sci. Eng., B134 (2006) 269.
20) L. J. Liu, S. Nakano, and K. Kakimoto, J. Cryst. Growth, 292 (2006) 515.
21) N. Miyazaki, Y. Kuroda, M. Sakaguchi, J. Cryst. Growth, 218 (2000) 221.
22) E. Orowan, Philos. T. Roy. Soc., A 52 (1940) 8.
23) J. Cochard, I. Yonenaga, S. Gouttebroze, M. M'Hamdi, Z. L. Zhang, J. Appl. Phys. 107 (2010) 033512.
24) M. Fukuzawa, M. Yamada, R. Islam, J. Chen, and T. Sekiguchi: J. Electron. Mater. 39 (2010) 700.
25) M. Yamada: Rev. Sci. Instrum. 64 (1993) 1815.
26) K. Jiptner, private communications.